Reprinted from JOURNAL OF THE ELECTROCHEMICAL SOCIETY
Vol. 131, No. 11, November 1984
Printed in U.S.A.
Copyright 1984

Wetting Angles and Surface Tension in the Crystallization of Thin Liquid Films

Eli Yablonovitch and Tom Gmitter

Exxon Research and Engineering Company, Annandale, New Jersey 08801

ABSTRACT

The behavior of thin liquid films is known to be dominated by surface tension forces. We show that the crystallization of thin liquid films requires that two wetting angle conditions be simultaneously satisfied: (*i*) relating to the liquid-vapor interface, and (*ii*) relating to the crystal-liquid interface. The balance between capillary pressure and thermal gradient forces shows that the equilibrium freezing point of thin films is actually depressed below the bulk freezing point. The magnitude of the effect is 1 K in an 800Å thick film. These observations suggest that small-scale thickness fluctuations may be responsible for the initiation of subgrain boundaries in the growth of crystalline silicon films.

The crystallization of thin liquid silicon films is a promising method (1) for producing single-crystal films of good electronic quality. These films will have important device applications in radiation hardening, dielectric isolation, high voltage integrated circuits, etc.

It is well known (2) that capillary forces, surface tension, and wetting play a vital role in the behavior of thin liquid films. In this article, we will derive the wetting angle requirements which permit the crystallization of thin liquid films to proceed. We will see that the success with liquid silicon films encapsulated in silicon dioxide is the result of a particularly fortuitous combination of wetting angles for those two materials.

Wetting Angle Requirements

In general, there is no assurance that a thin liquid film will be stable. There is the well-known tendency for the liquid film to "ball up" and form droplets on the surface of the substrate. The condition for spreading of the liquid film on a substrate is that its wetting angle should be identically zero. Since this is very rare, a different approach is used. We will show that a solid capping layer on the liquid film greatly relaxes this severe wetting angle constraint, and permits wetting under more easily satisfied conditions.

For practical stability, the liquid film should spread to fill any possible voids in the film, as shown in Fig. 1. Let

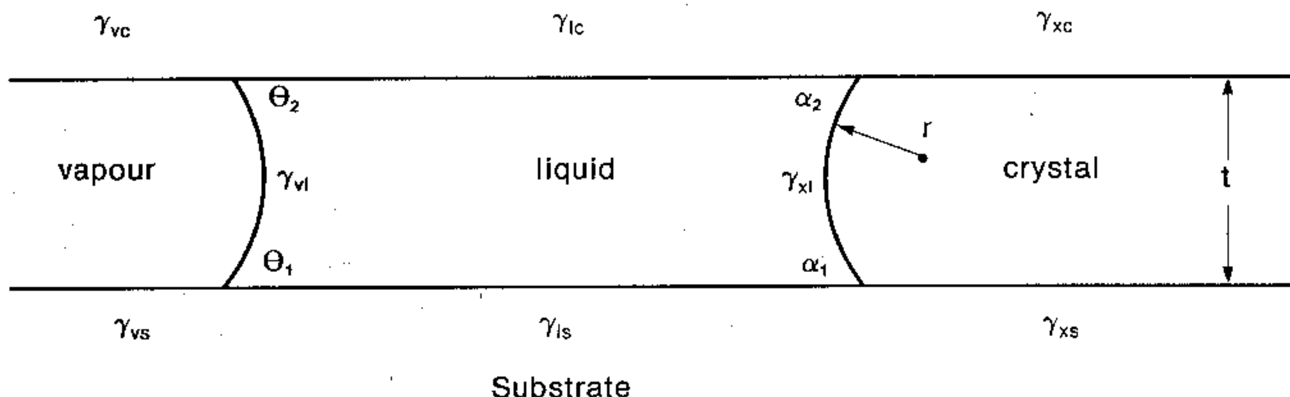

Fig. 1. A vertical cross-section through the thin liquid film. The liquid-vapor wetting angle, θ, is required to provide absolute stability against any voids which might be present in the film. The crystal-liquid angle α is required for high quality crystal growth and to prevent heterogeneous nucleation on the substrate. Note the radius of curvature r.

γ_{ls} and γ_{lc} be the surface energy (or tension) of the liquid with respect to the substrate and capping layer. Let γ_{vs} and γ_{vc} be the surface energy of the bare substrate and capping layer, respectively. The spreading of the liquid film should result in a net reduction of surface energy. Therefore

$$\gamma_{ls} + \gamma_{lc} - (\gamma_{vs} + \gamma_{vc}) < 0 \quad [1]$$

The Young-Dupre equation (2) for wetting angles, $\gamma_{vs} - \gamma_{ls} = \gamma_{vl} \cos \theta$, may be used to simplify inequality [1]

$$\cos \theta_1 + \cos \theta_2 > 0 \quad [2]$$

Inequality [2] states the wetting condition; the sum of the cosines of the wetting angles with respect to the substrate and the capping layer must be greater than zero. If the substrate and capping layer are made of the same material, then inequality [2] simply says that the wetting angle θ must be less than 90°. The wetting angle of liquid silicon on silica at the melting point has been independently measured (3) to be 87°, *i.e.*, barely within the regime of stability! This must be regarded as extremely fortuitous. Of course, without a capping layer we go back to the condition $\theta_1 = 0$, *i.e.*, wetting would be almost hopeless.

Since the surface tension γ_{vs} of the silica surface is thought to drop with increasing temperature, the angle θ_1 is thought (4) to become > 90° at temperatures 50-100 K above the silicon melting point. This probably explains the very narrow temperature window of stability in the crystallization of liquid silicon films on pure fused silica substrates. As a practical matter, it was found that the addition of a small amount of nitrogen (1) to the SiO_2 permitted the wetting conditions to be satisfied much more readily. The wetting angle of liquid silicon on Si_3N_4 is much less than 90°, having been measured (5) to be around 25°. It is understandable then that the addition of a small amount of Si_3N_4 to the SiO_2 might lower the wetting angle away from the condition of borderline stability, therefore broadening the temperature window of stability.

Thus far, we have considered wetting angles at the liquid-vapor interface, which controls the stability of the liquid film. Now we want to consider the crystal-liquid wetting angles, which will control the quality of crystal growth. It is a maxim (6) among crystal growers that the growth front should be convex away from the crystal. This permits any spurious crystal orientations to grow out to the edge and terminate there. A convex shape is guaranteed by wetting angles α_1 and α_2 both less than 90°. When α is greater than 90°, the Young-Dupre equation implies that γ_{xs}, the crystal-substrate interfacial energy, would be small, permitting easy heterogeneous nucleation of spurious grains at the surface of the substrate. In addition, the leading edge of the crystal growth would be a cusp at one or both interfaces. Good crystalline quality is inherently unstable at such a cusp.

Therefore, the wetting angle requirement for good crystalline quality is that the angle α_1 enclosed by the liquid at the interface between the crystal and the substrate should be less than 90°. Likewise, the angle α_2 with respect to the capping layer should be less than 90°.

Recently, Celler (8) observed the angle formed by liquid silicon between crystalline silicon and silica. The angle he observed is $60° < \alpha < 90°$, again fortuitously in the favorable range for good crystal growth. The two wetting angle conditions may now be summarized as (*i*) $\cos \theta_1 + \cos \theta_2 > 0$, and (*ii*) $\alpha_1 < 90°$ and $\alpha_2 < 90°$.

Capillary and Thermal Gradient Forces

The convex interface in Fig. 1 between the crystal and the liquid experiences a pressure due to its curvature. This is a type of capillary pressure which can be computed from the equation of Young and Laplace (2)

$$P = \gamma_{xl} \left[\frac{1}{r} + \frac{1}{R}\right] \quad [3]$$

where γ_{xl} is the interfacial tension between crystalline and liquid silicon, r is the radius of curvature in the plane of Fig. 1, and R is the radius of curvature in the orthogonal plane coming out of the page. The smaller radius, r, may also be written as $r = t/2 \cos \alpha$, where t is the thickness of the film.

If the growth front is straight (looking down at the film from above) then $R = \infty$. A top view of the growing crystal-liquid interface in Fig. 2(a) shows not that the growth front is straight, but, rather that it is scalloped. The growing front is made up of a series of curved sections joined at cusps. The grain boundaries between adjacent crystal domains meet the growth interface at the tip of the cusps, as indicated schematically in Fig. 2(b). Because of this scalloped structure, the convex radius of curvature R of each scallop is finite.

The structure we observe differs from the faceted structure seen in the beautiful photographs by Geis *et al.* (1). We have found that the structure of the crystallization front depends on the speed of growth. At low speeds, $\approx 10^{-3}$ cm/s, the growth front is scalloped, as shown in Fig. 2(a). At higher speeds, some fraction of the cusps become deep, V-shaped facets. As the growth speed increases, more of the cusps become faceted. At a speed of 3×10^{-2} cm/s, the entire growth front is faceted, similar to Fig. 6 of Ref. (1). The facets are <111> crystal faces which form because of the kinetic barrier against crystal growth on that face. When the sample scanning direction is reversed, the facets disappear, but the scalloped structure remains. The reversibility of the scalloped structure indicates that it is

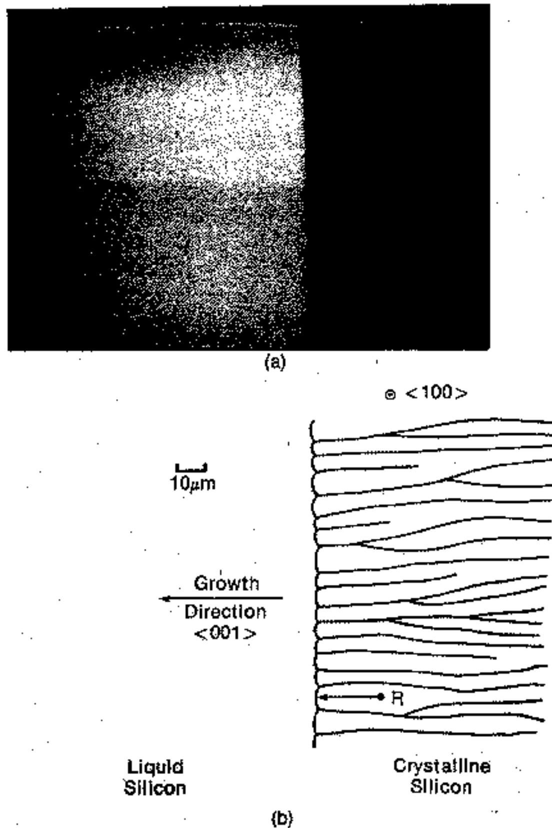

Fig. 2. (a) A video photograph of the crystal-liquid interface as seen in top view of the film. The crystal is the dark region on the right. Notice the presence of "scallops" on the growth front. The scallops join together at small pointed cusps, which are also seen on the growth front. (b) A schematic illustration of the grain boundary structure which might be visualized behind the growth front of Fig. 2(a). This grain boundary structure is typical of thin film crystal growth and has been observed in our experiments as well as others. It is implicit that the grain boundaries meet the growth front at the cusps. Note that R is the radius of curvature of a "scallop." A key question is: what is responsible for the nucleation of fresh grain boundaries in single-crystal material?

a minimum free energy configuration. In this article, we will explore mostly the regime of slow crystal growth. Nevertheless, we expect that many of the conclusions will apply equally well to more rapid crystal growth, where kinetic growth limitations begin to play a role.

In addition to the interfacial pressure due to the two radii of curvature r and R, Eq. [3], there is also a pressure term associated with the thermal gradient. Let z be the direction of crystal growth. The free energy associated with supercooling a layer of material of thickness dz is

$$\Delta G = \Delta S\,(T - T_m)\,dz\,dA \qquad [4]$$

where ΔS is the entropy of melting per unit volume, T_m is the melting temperature, and dA is the area of the growth front. Assuming a linear temperature gradient, $(T - T_m) = (z - z_m)dT/dz$, Eq. [4] may be rewritten as an equation for interfacial pressure

$$P = \Delta S \frac{dT}{dz}(z - z_m) \qquad [5]$$

where z_m defines the melting temperature isotherm. The pressure in Eq. [5] tends to push the crystal-liquid interface toward the position of the macroscopic melting point. That force is counteracted by the curvature pressure of the Young-Laplace Eq. [3], which pulls in the direction of supercooling. The actual amount of supercooling to be expected can be obtained by combining Eq. [3] and [5]

$$\Delta S \frac{dT}{dz}(z - z_m) = \gamma_{xl}\left[\frac{1}{r} + \frac{1}{R}\right] \qquad [6]$$

Equation [6] gives the balance between capillary pressure and thermal gradient forces. Of the two terms on the right-hand side, the most important is $1/r$, since it is largest. If the other term is temporarily neglected, and $r = t/2 \cos \alpha$, then Eq. [6] simplified to

$$\Delta S \frac{dT}{dz}(z - z_m) = \gamma_{xl}\frac{2\cos\alpha}{t} \qquad [7]$$

Equation [7] shows that the equilibrium freezing point is depressed by surface tension forces in thin films. This may be seen even more clearly by substituting for the right-hand side of Eq. [7] using the Young-Dupre equation

$$\Delta S \frac{dT}{dz}(z - z_m)\,t = 2(\gamma_{xs} - \gamma_{ls}) \qquad [8]$$

Equation [8] shows that the difference in surface free energy on the substrate between crystal and liquid is balanced by the volume free energy of supercooling. The equilibrium freezing point of thin films is therefore depressed by surface energy contributions. In the next section, we describe an experimental determination of the magnitude of this effect.

Freezing Point Depression

Equation [8] shows that fluctuations in thickness t can lead to variations in the positioning of the crystal growth front. Because of the importance of this phenomenon, we have made direct experimental confirmation of the effect and its magnitude.

In our experiment, thin films of silicon are deposited on top of fused quartz substrates and capped with SiO_2. As shown in Fig. 3, the substrates are heated from below by CO_2 laser radiation, and the melt front is observed from above by a high power optical microscope. Since SiO_2 is opaque to CO_2 laser radiation, the silicon films are heated only indirectly by conduction. A knowledge of the thermal conductivity of quartz and the gaussian mode parameters of the laser beam permits a calculation of the radial temperature distribution on top of the substrate. We observe the effect of thickness variations on the microscopic position of the melting front and the freezing front of the thin film. In order to make a more precise measurement, we found it advantageous for both a thick film and a thin film to be present simultaneously. The thick film was 7000Å of polycrystalline Si deposited by chemical vapor deposition (CVD). This was capped by 2000Å of CVD SiO_2. A second thin silicon layer only 800Å thick was then deposited and patterned by photolithography into stripes 35 μm wide. The whole structure was then capped again by 2000Å of CVD SiO_2. A cross section of the final structure is shown in Fig. 4(b). By making the upper layer

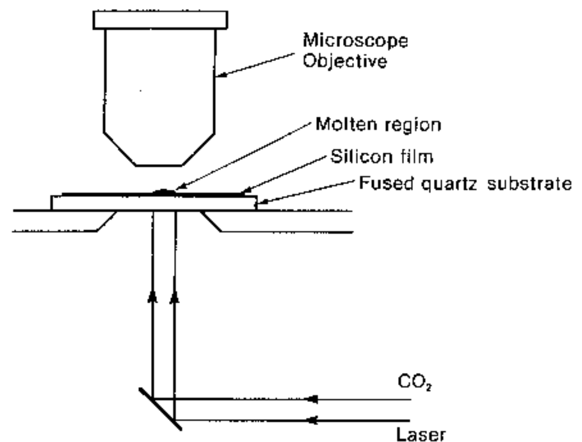

Fig. 3. The experimental arrangement used to produce the photographs in Fig. 2(a) and 4(a) was very simple. The CO_2 laser was fully absorbed in the fused quartz substrate, and the heating was by conduction.

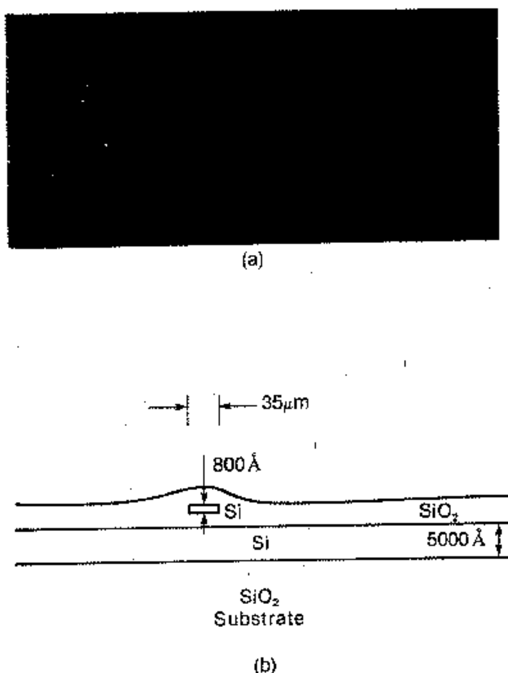

Fig. 4. (a) This photograph shows the depression of the freezing point in a thin film stripe in comparison to the thick film on which it rests. The dark region is crystalline silicon, and its crystallization front lags behind by approximately 1 K in the thin region relative to the thick region. The overall curvature is due to the round laser spot. (b) The cross section of the double layer structure of the film in Fig. 4(a). The Si, SiO_2, and Si layers were deposited in sequence. Then the thin silicon layer was patterned, and a final SiO_2 layer was applied.

in the form of narrow thin stripes, the position of the melt front in both the thin film and the thicker film can be observed simultaneously. Since the SiO_2 interlayer is only 2000Å thick, the temperature difference between the two films due to thermal radiation from the top surface is only 0.02 K, which is much smaller than the temperature shift we are seeking.

A micrograph of the position of the two crystallization fronts is shown in Fig. 4(a). The overall curvature of the growth front is indicative of the round melted spot produced by the laser beam. Away from the center of the melted region the temperature drops. From Fig. 4(a) the freezing point temperature is clearly lower in the thin stripe than in the thicker material beneath it.

The shift in the freezing point of the thin stripe relative to the thick film was a strong function of the thickness of the stripe. There was no shift if the stripe had the same thickness as the underlying thick film. As the stripe thickness was reduced, the temperature shift rose roughly as the reciprocal of thickness t, in good agreement with Eq. [7].

Owing to the opacity of the substrate to the CO_2 laser, strong thermal gradients are produced, and thermal conductivity rather than radiation is the dominant thermal transport mechanism. We present a calculation of the radial thermal conductivity of a disk heated by a gaussian laser beam in the Appendix to this article. The result of that calculation is that the radial temperature gradient is given by

$$\frac{dT}{dr} = \frac{2r}{\omega^2} \frac{K_{av}}{RK(T)} \Delta T \qquad [9]$$

where r is the radial distance from the center of the heated spot, ω is the gaussian radius of the laser beam, $K(T)/K_{av} = 1.17$ is the ratio of the thermal conductivity (9) of fused quartz at the melting point to the average thermal conductivity up to the melting point, $R = 2.02$ is the numerical value of an exponential integral, and ΔT is the overall temperature difference between the center of the heated spot and the edge of the fused quartz disk. The temperature gradient in Fig. 4(a) is approximately 0.15 K/μm.

As the molten zone in Fig. 4(a) was moved back and forth, for example by moving the sample relative to the laser beam, a hysteretic effect was observed, *i.e.*, the thickness-induced shift in freezing point was different from the corresponding shift in melting point. Upon freezing of a stripe about 800Å thick, the freezing point was depressed by 1 K relative to the thicker film beneath it. Upon remelting that same stripe, the melting point was virtually unchanged relative to the thicker film beneath it. Such hysteresis is common (2) in wetting angle measurements. An important distinction is therefore made between advancing wetting angles and receding wetting angles.

Such hysteresis is thought to be due to a change in surface energy of an interface due to its previous history. A freshly made crystal-SiO_2 interface has fairly high energy. After a period of time, there is probably significant reconstruction which lowers the surface energy. This may play the following role in our experiment. When the crystal advances into the liquid, it is forced to make a fairly energetic interface with the SiO_2, lowering the freezing point. When the liquid silicon advances into the crystal, it eliminates a low energy reconstructed crystal-SiO_2 interface. In that case, there is little or no melting point depression. Since we are interested in the crystallization of thin films, we will deduce the surface energies from freezing measurements rather than melting measurements.

Substituting the observed freezing point shift of thin stripes into Eq. [8] and using $\Delta S = 2.5$ J/K cm^3 for the entropy of melting, we obtain for $(\gamma_{xs} - \gamma_{ls})$ the value of 80-100 erg/cm^2. As far as we know, there are no previous measurements that this numerical value might be checked against.

There are two precautions that should be mentioned in making this measurement. At the melting temperature of silicon, amorphous SiO_2 is a glass with a finite viscosity and is not absolutely rigid. We found that it was necessary to complete the measurements fairly quickly (< 10s at the melt) in order to avoid severe thickness distortions of the thin stripe. The thickness was double-checked after freezing by profilometry and interferometry. The second precaution has to do with the initial melting of the polycrystalline film. As we have mentioned, there is little or no melting point depression of the crystallized film. Nevertheless, there is a large melting point depression of the as-deposited polycrystalline silicon. This is probably due to the excess free energy associated with the large grain boundary density in the as-deposited film. These observations, which monitor the initial polycrystalline film rather than the crystallized film, are not incorporated with the data in this paper. Only the results on the crystallized film are summarized in Table I.

Instability of the Crystallization Front

We have learned from the previous section that the freezing point is a function of film thickness. Equation [8] connects the film thickness with the position z of the crystal growth front. A local fluctuation in film thickness can cause the crystal growth front to move forward or backward locally relative to the rest of the front. The key question in thin film crystal growth is how to produce the largest possible single-crystal domains. In this

Table I. The hysteresis between freezing and melting is thought to be due to reconstruction of the crystalline silicon-SiO_2 interface, lowering its surface energy

	Temperature depression in an 800Å thick film relative to bulk ΔT	Surface energy difference with respect to SiO_2 substrate $(\gamma_{xs} - \gamma_{ls})$
Freezing	1 K	80-100 erg/cm^2
Melting	≈ 0 K	≈ 0 erg/cm^2

section, we suggest that locally concave regions of the growth front caused by local thickness fluctuations may be the birthplace of fresh subgrain boundaries. This would tend to limit the maximum possible crystal-domain size.

As indicated schematically in Fig. 2(b), and has been observed in virtually all thin film crystallization experiments, grain boundaries run together and recombine during crystal growth. Simultaneously, fresh grain boundaries initiate in previously single-crystal material. Both processes are shown schematically in Fig. 2(b), which is representative of typical (1, 10) photographs of grain boundary structure. It is the second of these two processes, the birth of fresh grain boundaries, which we must confront.

In the second section of this article, we mentioned the crystal grower's maxim (6) that the growth front should always be convex away from the crystal. It is very difficult to visualize how a fresh subgrain boundary may nucleate from single-crystal material. What we propose here is that concave regions of the growth front are the birthplace of fresh subgrain boundaries. In these regions, dislocations would tend to become locked into place and lead eventually to small-angle grain boundaries.

Although the growth front might be concave in top view, nevertheless, a cross-section view as shown in Fig. 1 would still remain convex, as demanded by the second wetting angle condition. Therefore, the actual three-dimensional geometry of that region is a saddle point. We are actually proposing that crystal growth at saddle points permits the initiation of small-angle grain boundaries.

As discussed in the third section and shown in Fig. 2(a), the growth front itself is scalloped, meeting the pre-existing subgrain boundaries at cusps. Each scallop represents a single crystal domain and has a finite radius of curvature R. This convex curvature tends to stabilize the domain structure and inhibit the birth of fresh subgrain boundaries. A local thickness fluctuation will have no effect unless it is deep enough to retard the growth front sufficiently to change it from convex curvature to locally concave. If the scallop radius of curvature R is very small, it would take an extremely deep and spatially localized thickness fluctuation to change it from convex to concave. Conversely, if the scallop is wide, representing a large crystal grain, the scallop radius of curvature R is large indicating a relatively straight growth front. In that case, even a small thickness fluctuation can change R from convex to concave. Thus, large grains are relatively unstable to grain boundary nucleation and they tend to split in two. Meanwhile, small grains tend to be stable and to avoid further subdivision. Therefore, the grain boundary structure represented in Fig. 2(b) tends to be stabilized around a certain crystal-domain width.

In conclusion, we have shown that thickness fluctuations could be responsible for the initiation of subgrain boundaries by producing locally concave regions of the growth front. A scalloped growth front, consisting of a series of domains of convex curvature, tends to be stable against growth front fluctuations. The balance between these two tendencies produces the actual grain structure that is observed.

Conclusions

The crystallization of thin liquid films demands that two wetting angle conditions be simultaneously satisfied: (*i*) regarding the liquid-vapor interface on the substrate, and (*ii*) regarding the crystal-liquid interface on the substrate.

The position of the crystal growth interface is determined by the balance between capillary forces, which tend to push the growth front to temperatures below the bulk freezing point, and thermal gradient forces which tend to pull the growth front toward the freezing point. The balance between these forces results in an equilibrium depression of the freezing point of thin films of about 1 K for an 800Å thick film. This implies a surface tension difference ($\gamma_{xs} - \gamma_{ls}$) of approximately 80-100 erg/cm^2.

The coupling between thickness and growth front position provides a mechanism for a crystal-growth instability. Thickness fluctuations can produce locally concave regions of the growth front, where subgrain boundaries could initiate. The convex curvature of the scalloped growth front counteracts this effect and tends to stabilize the crystal domain structure.

Acknowledgments

We gratefully acknowledge the assistance of Mike Schneider, Bob Weinberger, Harry Deckman, and John Dunsmuir. We also thank Professor Hank Smith for his comments on the manuscript.

Manuscript received April 23, 1984.

Exxon Research and Engineering Company assisted in meeting the publication costs of this article.

APPENDIX

In this Appendix, we derive the thermal gradient produced in a thermally conducting disk by a gaussian laser beam. The CO_2 laser is absorbed within 10 μm of the surface of fused quartz. In principle, both conduction and radiation could play a role in transporting this heat. For the t = 0.75 mm thickness fused quartz plates used in these experiments, radial thermal conduction plays the major rôle, owing to the strong thermal gradient induced by the laser beam with radiative heat loss being only a small correction.

The power per unit area absorbed from a gaussian laser beam is

$$P(r) = \frac{2P_0}{\pi\omega^2} \exp\left\{-\frac{2r^2}{\omega^2}\right\}$$

where ω is the gaussian radius of the laser beam, about 2.8 mm in our case. P is its total power, about 30W and r is the distance from the central axis of the beam. The total power inside a spot of radius r is

$$H(r) = P_0\left(1 - \exp\left\{-\frac{2r^2}{\omega^2}\right\}\right)$$

The thermal conduction equation in the radial direction is

$$H(r) = \frac{K(T)\, 2\pi rt\, dT}{dr} \quad \text{[A-1]}$$

where $K(T)$ is the temperature dependent thermal conductivity of fused quartz. Integrating Eq. [A-1] yields

$$\frac{P_0}{2\pi t}\int_0^r \left(1 - \exp\left\{-\frac{2r^2}{\omega^2}\right\}\right)\frac{dr}{r} = \int_{T_{max}}^{T_{min}} K(T)\, dT \quad \text{[A-2]}$$

The integral in Eq. [A-2] is an "Exponential Integral," which is (11) approximately $R = [\ln(2r^2/\omega^2) + 0.577]/2 =$ 2.02 in our geometry. Let us write the difference between the temperature T_{max} at the center of the laser spot and T_{min} the temperature at the edge of the fused quartz disk as $\Delta T = T_{max} - T_{min}$. Then the integrated heat flow equation can be written

$$\frac{P_0}{2\pi t} = \frac{K_{av}\,\Delta T}{2.02} \quad \text{[A-3]}$$

Simplifying [A-1] by taking $r < \omega$ we obtain

$$\frac{dT}{dr} = \frac{P_0}{2\pi t}\frac{2r}{K(T)\,\omega^2} \quad \text{[A-4]}$$

Substituting [A-4] in [A-3]

$$\frac{dT}{dr} = \frac{2r}{\omega^2}\frac{K_{av}}{RK(T)}\Delta T$$

which is the same as Eq. [9] in the text.

REFERENCES

1. M. W. Geis, H. I. Smith, D. J. Silversmith, R. W. Mountain, and C. V. Thompson, *This Journal*, **130**, 1178 (1983).
2. A. W. Adamson, "Physical Chemistry of Surfaces," Third ed., John Wiley and Sons, New York (1976).

3. K. M. Kim, S. Berkman, H. E. Temple, and G. W. Cullen. *J. Cryst. Growth*, **50**, 212 (1980).
4. S. Berkman, Private communication.
5. T. J. Whalen and A. T. Anderson, *J. Am. Ceram. Soc.*, **58**, 396 (1975); E. Kuroda, M. Matsuda, and M. Maki, *Phys. Status Solidi A*, **48**, 105 (1978).
6. J. C. Brice, "The Growth of Crystals from Liquids," see especially p. 209, North-Holland, Amsterdam (1973).
7. D. P. Woodruff, "The Solid-Liquid Interface," see especially p. 31, Cambridge University Press, London (1973).
8. G. K. Celler, Private communication.
9. "Handbook of Thermophysical Properties of Solid Materials," Vol. III, "Ceramics," A. Goldsmith, T. E. Waterman, and H. J. Hirschhorn, Editors, see especially p. 893, Pergamon Press, New York (1961).
10. M. W. Geis, H. I. Smith, B. Y. Tsaur, J. C. C. Fan, D. J. Silversmith, and R. W. Mountain, *This Journal*, **129**, 2812 (1982).
11. M. Abramowitz and I. A. Stegun, "Handbook of Mathematical Functions," see especially p. 228, Dover, New York (1965).